Journal of Medicinal Chemistry

pubs.acs.org/jmc

Article

Discovery and Optimization of a 4-Aminopiperidine Scaffold for Inhibition of Hepatitis C Virus Assembly

Adam Rolt,[⊥] Daniel C. Talley,[⊥] Seung Bum Park, Zongyi Hu, Andrés Dulcey, Christopher Ma, Parker Irvin, Madeleine Leek, Amy Q. Wang, Andrew V. Stachulski, Xin Xu, Noel Southall, Marc Ferrer, T. Jake Liang, and Juan J. Marugan*

Cite This: *J. Med. Chem.* 2021, 64, 9431−9443

Read Online

ACCESS | Metrics & More | Article Recommendations | Supporting Information

ABSTRACT: The majority of FDA-approved HCV therapeutics target the viral replicative machinery. An automated high-throughput phenotypic screen identified several small molecules as potent inhibitors of hepatitis C virus replication. Here, we disclose the discovery and optimization of a 4-aminopiperidine (4AP) scaffold targeting the assembly stages of the HCV life cycle. The original screening hit (1) demonstrates efficacy in the HCVcc assay but does not show potency prior to or during viral replication. Colocalization and infectivity studies indicate that the 4AP chemotype inhibits the assembly and release of infectious HCV. Compound 1 acts synergistically with FDA-approved direct-acting antiviral compounds Telaprevir and Daclatasvir, as well as broad spectrum antivirals Ribavirin and cyclosporin A. Following an SAR campaign, several derivatives of the 4AP series have been identified with increased potency against HCV, reduced *in vitro* toxicity, as well as improved *in vitro* and *in vivo* ADME properties.

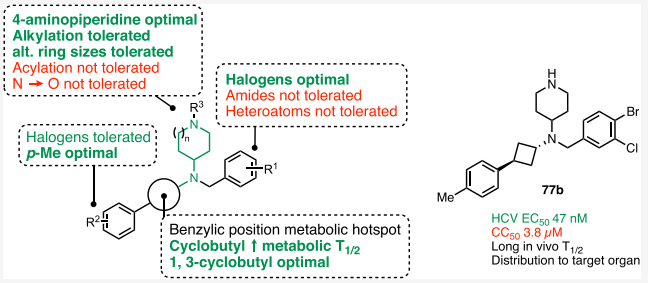

INTRODUCTION

Hepatitis C virus (HCV) is a small, single-stranded, positive-sense RNA virus that infects more than ∼70 million people worldwide.[1] As a consequence, upwards of 399 000 deaths per year are associated with acute HCV infection.[2] Acute HCV infection, while initially asymptomatic, can progress to chronic infection, resulting in hepatocellular carcinoma, cirrhosis, and liver failure. There are now several approved drugs and combination therapies for the treatment of HCV;[3] all combination therapies are currently composed of direct-acting antivirals (DAAs) that inhibit various HCV nonstructural (NS) proteins. Harvoni (Gilead Sciences), a combination therapy of Ledipasvir/Sofosbuvir targeting NS5A and NS5B, respectively, was first approved for use in late 2014. Several clinical trials have demonstrated promising anti-HCV efficacy, with >90% of patients achieving a sustained viral response 12 weeks post treatment (SVR_{12}) across most HCV genotypes; however, the response in genotype 3 was lower (82%).[4−7] The combination therapies Viekira Pak (XR) and Technivie (Abbvie) are composed of Paritaprevir/Ombitasvir/Dasabuvir (± Ritonavir) targeting NS3/4A, NS5A, and NS5B respectively; these regimes also demonstrate efficacy across several genotypes with high SVR_{12} rates.[8−10]

The impact of a new therapeutic intervention can be framed as a product of both efficacy and accessibility; it has been noted that while the SVR_{12} per treatment course has improved, the cost per SVR_{12} has not, and so the cost per treatment course has increased drastically in line with the efficacy of modern combination therapies.[11] The average wholesale price of a 12 week treatment course is approximately $100 000 USD for both options mentioned above,[3] resulting in a large financial burden on healthcare systems in more economically developed countries.[12] Combination therapies comprising drugs with synergistic modes of action are often highly efficacious due to the enhanced ability to overcome robustness in biological networks or other compensatory mechanisms.[13] This can reduce total treatment cost, treatment duration, and improve adherence by overcoming dose-limiting toxicity, ultimately improving the impact of these therapies. Specifically, in the context of infectious disease, coadministration of multiple compounds with different modes of action can prevent viral rebound by raising the evolutionary barrier required to develop resistance.[14] To this end, we recently reported on the discovery,[15] optimization,[16] and preclinical pharmacological development[17] of analogues of the FDA-approved antihistamine drug chlorcyclizine (CCZ), as well as the discovery, optimization,[18] and efficacy evaluation of

Received: April 16, 2021
Published: June 29, 2021

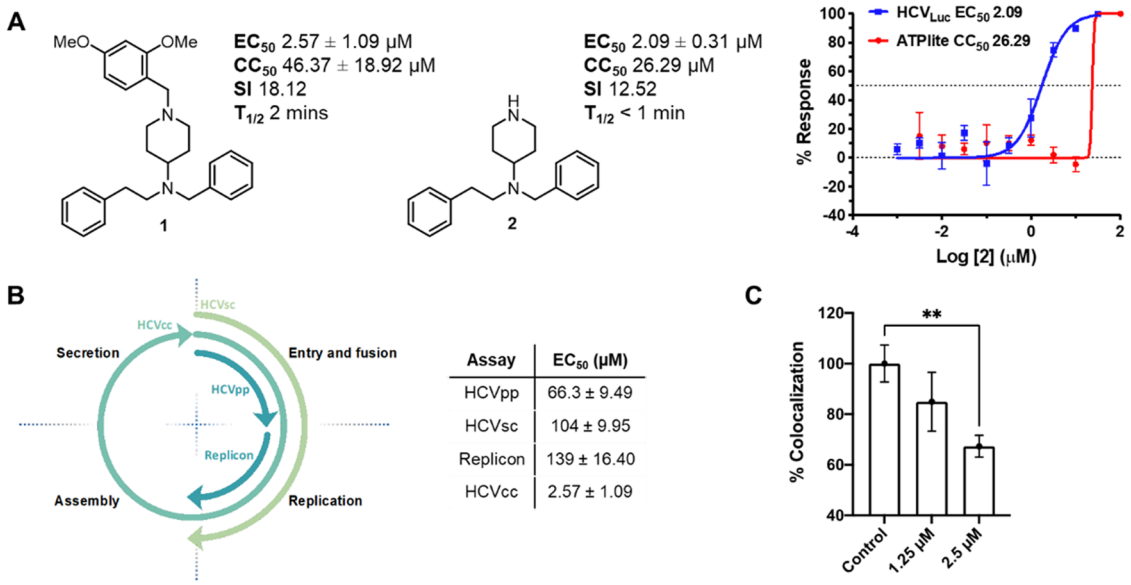

Figure 1. (A) Structure and key properties of hit molecules 1 and 2, and a representative dose−response curve for compound 2. (B) Schematic representation of the portion of the HCV life cycle which is represented in the given assays. The adjacent table reports the effective concentration (EC_{50}) of compound 1 in these assays—comparative efficacy is used to inform mechanism of action studies. HCVsc—HCV single cycle, HCVpp—HCV pseudoparticles, and HCVcc—HCV cell culture. (C) Compound 1 disrupts the colocalization of HCV core proteins with cytosolic lipid droplets during virus assembly in immunofluorescence experiments in a dose-dependent manner, see also Supplemental Figure 1. Student's *t*-test *P*-value = 0.0026 (**).

Fluoxazolevir.[19] Both series target the HCV glycoprotein E1 and interfere with the fusion process between HCV and the inner endosomal membrane during the entry process.[20]

Following viral entry and replication, the late stages of the HCV life cycle (such as assembly, trafficking to the cell surface, and secretion), represent complex multifactorial processes that have yet to be fully elucidated. Individual factors and processes that are known to be involved in HCV assembly have been modulated as potential therapeutic targets, but unfortunately have yet to be truly leveraged as an antiviral therapy.[21−25] Here, we describe our work in the discovery and optimization of a novel class of HCV assembly inhibitors with hopes to improve upon the current treatment regimes. The original hit **1** was optimized in a medicinal chemistry campaign, resulting in increased potency against HCV, reduced *in vitro* toxicity, as well as improved *in vitro* ADME properties. Pharmacokinetic studies in mice show favorable liver distribution with a long metabolic half-life and importantly, no observed changes in behavior or acute toxicity.

RESULTS

Identification of 4-Aminopiperidines as Modulators of HCV Assembly. Following the development and validation of a HCVcc qHTS platform by Hu and colleagues[26] utilizing an HCV construct harboring a luciferase reporter in the p7 region (HCV-Luc), a screen of the NIH Molecular Libraries Small Molecule Repository (MLSMR, 339 561 compounds)[27,28] led to the identification of 4-aminopiperidine (4AP) derivatives, **1** and **2**, as potent inhibitors of HCV proliferation (EC_{50} values of 2.57 and 2.09 μM, respectively) (Figure 1A). Compounds **1** and **2** did not show appreciable toxicity in an ATPlite counter screen (CC_{50} > 20 μM). The physicochemical/*in vitro* ADME properties (parallel artificial membrane permeability, solubility in aqueous buffer, and stability in rat liver microsome lysates) of these compounds were determined. Permeability and solubility were quite promising, but potential metabolic liabilities were revealed in rat liver lysates ($T_{1/2}$ < 2 min). Potency and metabolic stability were flagged as key metrics for improvement moving forwards to medicinal chemistry.

By studying the effects of compound **1** in different HCV infection systems, the specific stage of the viral life cycle upon which the series acts can be determined (Figure 1B). HCV pseudoparticles (HCVpp)[29] consist of HCV entry glycoproteins (E1 and E2) incorporated into the surface of a lentivirus core, which bind to and enter hepatocytes in the same manner as HCV. As such, HCVpp can be used to study the effect of a small molecule specifically on viral entry. The HCV single-cycle assay (HCVsc)[30] utilizes a defective virus particle that can enter hepatocytes, undergo fusion, and replicate but cannot assemble into infectious viral particles, which permits the distinction of pre/postreplication inhibition. The HCV subgenomic replicon system (replicon assay) can be used to study the steps involved specifically in the replication of the virus. Finally, the HCV cell culture system (HCVcc) can be used, which captures the full virus life cycle; HCV particles will enter the cells, replicate, and assemble to form infectious HCV particles, which are then secreted into the extracellular milieu.

Evaluation of compound **1** in these various assays reveals effective inhibition of HCV life-cycle progression only in stages following viral replication. HCVpp, HCVsc, and the replicon assay all report low activity (EC_{50} > 50 μM) in comparison to that observed in the HCVcc system (EC_{50} 2.03 μM); these data suggest that **1** inhibits HCV replication in either the assembly or secretion stages (Figure 1B, left).

Following translation on the endoplasmic reticulum (ER), HCV core proteins are trafficked to cytosolic lipid droplets (cLD's) where they remain until viral assembly, which takes place at the ER/cLD interface.[29,31,32] The association between HCV core proteins and cLDs can be quantified by immunofluorescence; compound **1** was found to inhibit the colocalization of HCV core and cLDs in a dose-dependent

https://doi.org/10.1021/acs.jmedchem.1c00696
J. Med. Chem. 2021, 64, 9431−9443

Table 1. Levels of Synergy of (1) with Previously Identified and FDA-Approved Inhibitors of HCV

	ribavirin	telaprevir	daclatasvir	2′-*C*-methylcytidine	cyclosporin A
level of synergy[a]	+++	+++	+++	+++	+

[a]Extent of synergy or antagonism in MacSynergy II is defined according to absolute value of log volume (LV): (+++), LV > 9, major synergy; (++), 5 < LV < 9, moderate synergy; and (+) 2 < LV < 5, minor synergy.

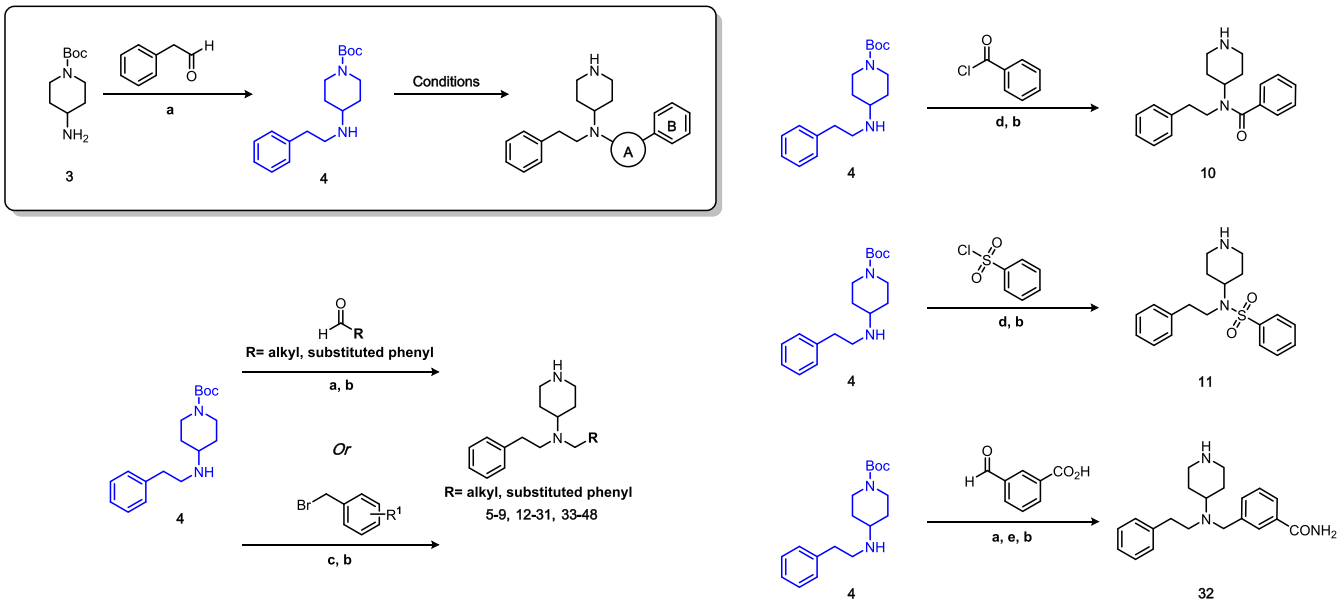

Figure 2. Overview of synthetic methods used in the first round of SAR exploring linker region **A** and phenyl ring **B** to generate compounds **5**−**54** (a) $NaBH(OAc)_3$, DCE, RT. (b) 4N HCl/dioxane (c) K_2CO_3, THF, 60 °C. (d) NEt_3, DCM, RT. (e) NH_4Cl, HATU, DIPEA, and DMF.

Table 2. Initial Exploration of Linker A and Phenyl Ring B[a]

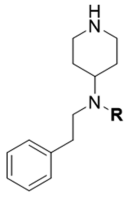

ID	R	EC_{50} (μM)	CC_{50} (μM)	SI	$T_{1/2}$	ID	R	EC_{50} (μM)	CC_{50} (μM)	SI	$T_{1/2}$
5		>35	>100	ND	ND	11	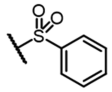	>35	>100	ND	1.40
6	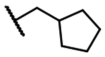	1.16 ± 0.16	24.5 ± 1.62	21.1	1.7	12	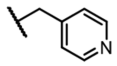	>35	>100	ND	3.6
7	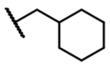	1.37 ± 0.98	7.32 ± 0.68	5.34	1.9	13	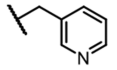	>35	>100	ND	<1
8	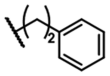	1.48 ± 0.05	19.54 ± 6.56	13.2	1.70	14	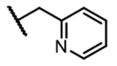	>35	>100	ND	1.8
9	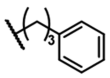	2.82 ± 0.46	9.18 ± 0.18	3.25	<1	15	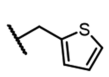	3.98 ± 1.76	31.96	8.0	<1
10	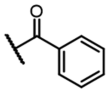	>35	>100	ND	1.60	16	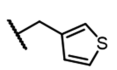	3.84 ± 1.25	ND	ND	<1

[a]EC_{50} and CC_{50} are the averages of three independent measurements, which were each performed in triplicate. Absolute values are reported alongside standard deviation. >35 and >100 indicate that the values lie outside of the maximum concentrations tested for efficacy and cytotoxicity, respectively. SI = selectivity index (CC_{50}/EC_{50}) $T_{1/2}$ = metabolic half-life measured in rat liver microsomes reported in minutes, the minimum detectable half-life of 1 min.

https://doi.org/10.1021/acs.jmedchem.1c00696
J. Med. Chem. 2021, 64, 9431−9443

Table 3. Further Exploration of SAR Around Phenyl Ring B

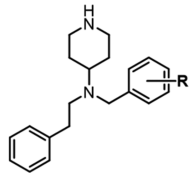

ID	R	EC_{50} (μM)	CC_{50} (μM)	SI	$T_{1/2}$	ID	R	EC_{50} (μM)	CC_{50} (μM)	SI	$T_{1/2}$
2	H	2.10 ± 0.31	26.29	12.5	<1	**28**	*m*-CF_3	1.80 ± 0.37	4.35 ± 0.32	2.4	1.9
17	*p*-Cl	1.36 ± 0.29	6.36 ± 1.74	4.7	3.7	**29**	*m*-OCF_3	3.75 ± 1.08	ND	ND	<1
18	*p*-Br	1.63 ± 0.28	4.53 ± 0.13	2.8	4.6	**30**	*m*-Me	3.66 ± 0.55	5.4 ± 0.063	1.5	<1
19	*p*-F	0.92 ± 0.52	56.49 ± 43.50	61.0	1.9	**31**	*m*-NHAc	>35	>100	ND	1.7
20	*p*-CF_3	1.06 ± 0.30	4.74 ± 0.02	4.5	12.7	**32**	*m*-$CONH_2$	>35	>100	ND	<1
21	*p*-OCF_3	1.29 ± 0.69	ND	ND	6.7	**33**	*o*-Cl	1.40 ± 0.18	4.4 ± 0.11	3.1	2.1
22	*p*-OMe	2.48 ± 0.33	25.24 ± 5.43	10.2	2	**34**	*o*-Br	2.19 ± 0.77	4.56 ± 1.97	2.1	<1
23	*p*-Me	3.88 ± 0.79	4.86 ± 0.14	1.3	2.3	**35**	*o*-F	5.22 ± 0.49	ND	ND	1.7
24	*p*-CN	7.4 ± 2.14	27.3 ± 0.03	3.7	2.9	**36**	*o*-CF_3	2.60 ± 0.97	4.65 ± 0.88	1.8	1.4
25	*m*-Cl	0.45 ± 0.13	4.55 ± 0.15	10.1	1.6	**37**	*o*-OMe	1.75 ± 0.37	20.80 ± 5.66	12.2	<1
26	*m*-Br	0.97 ± 0.19	6.40 ± 1.60	6.6	2.8	**38**	*o*-NHAc	>35	>100	ND	3
27	*m*-F	1.21 ± 0.31	8.89 ± 4.01	7.3	1.8						

Table 4. Final Round of Exploration of SAR Around Phenyl Ring B—Disubstituted Halogen Analogues

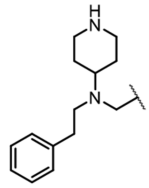

ID	R	EC_{50} (μM)	CC_{50} (μM)	SI	$T_{1/2}$	ID	R	EC_{50} (μM)	CC_{50} (μM)	SI	$T_{1/2}$
39	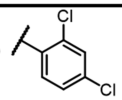	0.48 ± 0.14	5.15 ± 0.76	10.7	2.2	**44**	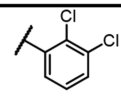	2.3 ± 0.04	4.82 ± 0.44	2.1	30
40	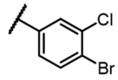	0.21 ± 0.04	5.77 ± 0.13	27.4	2.6	**45**	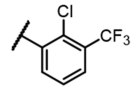	1.74 ± 0.45	6.21 ± 0.94	3.6	2.1
41	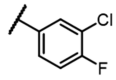	1.09 ± 0.13	5.26	4.8	2	**46**	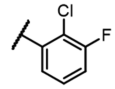	3.42	6.65 ± 0.74	1.9	ND
42	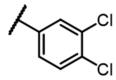	1.57 ±	7.03 ± 1.12	4.47	2.4	**47**	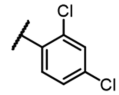	0.93 ± 0.21	15.38 ± 10.11	16.5	3
43	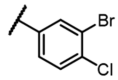	1.74 ± 0.7	6.77 ± 1.50	3.89	2.4	**48**	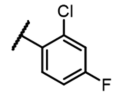	1.82 ± 0.06	4.92 ± 0.35	2.7	ND

manner (Supporting Information, Figure 1), with approximately 70% inhibition at 2.5 μM (Figure 1C). Taken together with compartmentalized life-cycle efficacy studies (Figure 1B), hit compounds **1** and **2** appear to specifically inhibit HCV assembly, potentially by interrupting the trafficking or localization of HCV core proteins onto cLDs.

We set out to evaluate potential synergism between **1** and representative compounds from different classes of previously identified HCV inhibitors. The HCV-Luc assay, used for our HTS in parallel with the ATPlite assay for cytotoxicity, was performed in dose response using combinations of **1** and various concentrations of each FDA-approved drug. The levels of synergy were calculated using the MacSynergy II software[33] according to the Bliss independence model (Table 1). Compound **1** showed significant synergism with ribavirin, telaprevir (NS3/4A inhibitor), daclatasvir (NS5A inhibitor), and 2′-*C*-methylcytidine (NS5B inhibitor). Minor synergism was shown with cyclosporin A. No significant *in vitro* cytotoxicity was observed in any of these assays, which strongly supports the use of this chemotype in combination with previously approved anti-HCV drugs from a pharmacodynamic perspective.

Synthesis. Given both the unique mechanism of action and synergistic effects with approved HCV therapeutics, a medicinal chemistry campaign was conducted to improve upon anti-HCV activity and ADME properties of this chemotype (predicted using *in vitro* ADME/physicochemical

https://doi.org/10.1021/acs.jmedchem.1c00696
J. Med. Chem. 2021, 64, 9431−9443

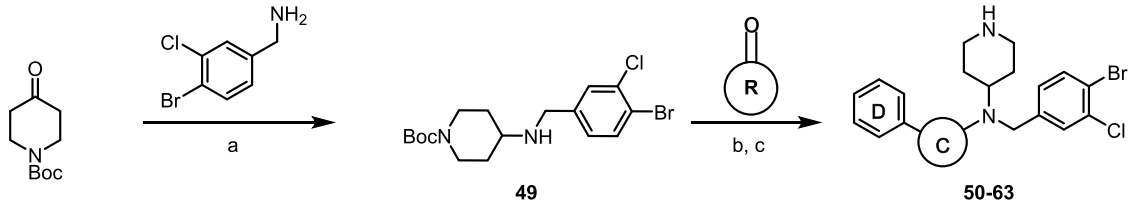

Figure 3. Synthetic route and exploration of SAR around linker **C** and corresponding phenyl ring **D** (a) AcOH, $NaBH(OAc)_3$, DCE, RT. (b) AcOH, DCE, 60 °C, then $NaBH(OAc)_3$. (c) 4N HCl/dioxane, RT.

properties and later evaluated via pharmacokinetic studies in mice).

The synthesis of the first round of analogues in the 4AP series is outlined in Figure 2; this round consists of a broad exploration of tolerated functionality in linker "A" and the connected aryl ring, "B" as shown. Reductive amination of 4-amino-1-Boc-piperidine, **3**, with 2-phenylacetaldehyde yields common intermediate **4**, which is then used in the preparation of various analogues in a two-step procedure involving coupling with an appropriate electrophile and subsequent Boc-deprotection. These methods facilitated the systematic exploration of a wide variety of analogues (Figure 2, Tables 2−4). Compounds **5**−**9**, **12**−**31**, and **33**−**48** were prepared either using triacetoxyborohydride-mediated reductive amination or alkylation with alkyl bromides, followed by acidic Boc-deprotection (method was chosen predominantly based on in-house availability of building blocks). Amide **10** and sulfonamide **11** were prepared in similar fashions, acylation with benzoyl chloride or sulfonylation with benzenesulfonyl chloride under basic conditions, then subsequent Boc-deprotection furnishes the respective N-substituted compounds. Amide analogue **32** was synthesized via reductive amination with the appropriate 3-formylbenzoic acid, followed by HATU-mediated amide coupling with ammonium chloride and excess base, followed by Boc-deprotection.

Subsequent rounds of SAR were conducted in a similar fashion (Figure 3); *tert*-butyl 4-oxopiperidine-1-carboxylate was coupled to 4-bromo-3-chlorobenzaldehyde via reductive amination yielding common intermediate **49**, facilitating exploration about Ring "D" and the respective linker "C" (Table 5a). A 1,3-cyclobutane linker was found to be optimal, so additional analogues about Ring "D" were synthesized retaining this linker (Table 5b).

After thoroughly investigating this spacer and the substituents about the phenyl ring, compound **65** is synthesized retaining all previously optimized structural features (1,3-cyclobutane linker and *p*-methylphenyl), for an SAR exploration about the piperidine ring (Figure 4; Table 6). Importantly, this particular synthetic route allowed for the separation of cyclobutyl linker *cis*- and *trans*-diastereomers of compound **65** after the first step, permitting the synthesis of *trans*-**76a** and *cis*-**76b** in a selective manner (Figure 5; Table 7). Diastereomers after the final transformation were inseparable under all chiral column purification conditions tested and so must be purified at this stage.

SAR Studies. The anti-HCV efficacy is determined in the HCV-Luc assay system[34] and is reported as EC_{50}; the concentration of compound giving a 50% reduction in luciferase signal measured in triplicate. Cytotoxicity was determined concomitantly using the ATPLite cytotoxicity assay and is reported as CC_{50}; the concentration of compound exhibiting 50% cytotoxicity measured in triplicate. Both

Table 5a. Exploration about the Linker "C" (as Designated in Figure 3)

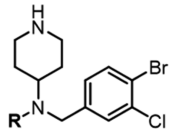

ID	R	EC_{50} (μM)	CC_{50} (μM)	SI	$T_{1/2}$
50	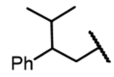	2.55 ± 1.38	3.39 ± 1.87	0.56	23.26
51	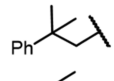	1.77 ± 0.18	5.15 ± 0.76	0.92	15.4
52	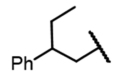	0.81 ± 026	2.96 ± 1.76	2.20	ND
53	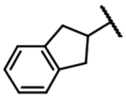	0.89 ± 0.31	6.28 ± 0.99	2.68	13.86
54		2.57 ± 0.19	18.69	6.76	1.89
55	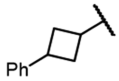	0.48 ± 0.22	3.79 ± 0.48	4.87	12.25

measurements are normalized to vehicle (DMSO) controls; 0% inhibition of HCV and 0% cytotoxicity, respectively. Throughout the medicinal chemistry campaign, the physicochemical/*in vitro* ADME properties were also determined including partial artificial membrane permeability (PAMPA) at pH 7.4, solubility in aqueous buffer, and stability in rat liver microsome lysates. For most synthetic analogues, only the rat liver microsomal stability ($T_{1/2}$) is shown in the tables, as this is the only physicochemical/metabolic parameter which required significant optimization for the chemotype ($T_{1/2}$ < 2 min for both **1** and **2**). However, all *in vitro* ADME data can be found in the Supporting Information.

By comparing the activity of compounds **1** and **2** (Figure 1A), it is clear that the piperidinyl *N*-benzylic moiety did not significantly impact the potency of the compound. As such, it was excluded from the scaffold moving forward and compound **2** was used as a benchmark in the SAR study.

Linker "A" (as shown in Figure 2) was the first region to be explored while maintaining the unsubstituted piperidine and the phenethyl moieties (Table 2). Lengthening the carbon-linker from the central tertiary amine to the phenyl ring from methylene (hit **2**), to ethylene (**8**), or propylene (**9**), does not have a strong effect on efficacy. Substitution of the side chain for *sec*-butyl (**5**) abolishes activity (EC_{50} > 35 μM); however,

https://doi.org/10.1021/acs.jmedchem.1c00696
J. Med. Chem. 2021, 64, 9431−9443

Table 5b. Additional Exploration about the "D" Phenyl Region and *In Vitro* ADME Properties

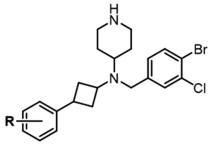

					ADME[a]		
ID	R	EC_{50} (μM)	CC_{50} (μM)	SI	$T_{1/2}$	PAMPA (1×10^{-6} cm/s)	solubility (μg/mL)
56	*p*-Me	0.075 ± 0.034	4.82 ± 0.45	64.23	>30	806	18.17
57	*p*-Cl	3.54 ± 1.06	71.31 ± 28.69	20.14	>30	ND	ND
58	*p*-Br	0.19 ± 0.06	3.63 ± 1.64	19.1	28.49	32	3.32
59	*p*-F	0.60 ± 0.06	4.78 ± 0.09	7.9	11.81	398	ND
60	*m*-Me	0.38 ± 0.19	4.95 ± 0.31	13	ND	265	ND
61	*m*-Cl	0.13 ± 0.02	4.06 ± 0.63	31.2	23.94	ND	4
62	*m*-Br	0.72 ± 0.29	4.72 ± 1.19	6.5	19.3	14	3.94
63	*m*-f	1.12 ± 0.02	5.07 ± 0.19	4.52	18.91	ND	ND

[a]ADME (*in vitro*; physicochemical) parameters: $T_{1/2}$ = metabolic half-life measured in rat liver microsomes reported in minutes, minimum detectable half-life of 1 min. Parallel artificial membrane permeation assay (PAMPA) is reported as a metric of the passive permeability of the compounds (1×10^{-6} cm/s). Solubility—pION μSOL assay for kinetic aqueous solubility determination, pH 7.4.

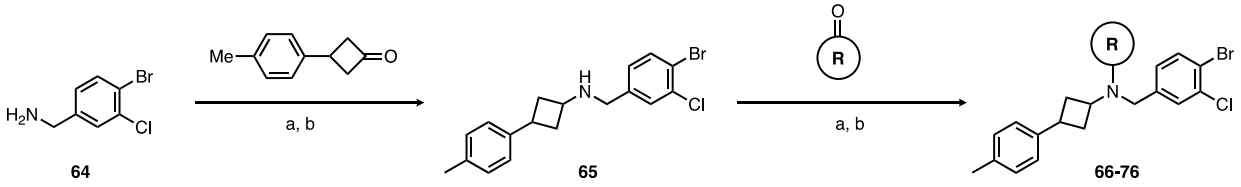

Figure 4. Synthesis of analogues about "piperidine region" **R**. (a) AcOH, DCE, 60 °C, then $NaBH(OAc)_3$, RT. (b) 4N HCl/dioxane, RT.

Table 6. Biological Activity and ADME Properties for Analogues about Piperidine Ring

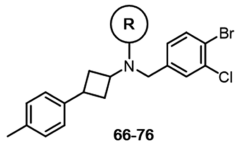

					ADME								ADME		
ID	R	EC_{50} (μM)	CC_{50} (μM)	SI	$T_{1/2}$	PAMPA ($1e^{-6}$ cm/s)	Solubility (μg/mL)	ID	R	EC_{50} (μM)	CC_{50} (μM)	SI	$T_{1/2}$	PAMPA ($1e^{-6}$ cm/s)	Solubility (μg/mL)
66		>35	>35	ND	3.67	<6.4	<1	**72**		0.76	>35	>46.1	<30	665.84	25.62
67		>35	>35	ND	6.73	1909	<1	**73**		3.43	>35	>10.2	12.2	ND	23.2
68	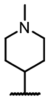	0.32	>35	>109.3	14.05	274.27	22.94	**74**		1.26	>35	>27.7	<30	122.99	7.26
69	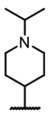	0.20	>35	>175	17.36	<23.1	15.39	**75**	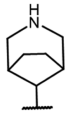	1.17	11.20	9.3	<30	ND	<1
70	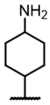	0.30	>35	>116.6	<30	818.04	ND	**76**		0.93	10.01	10.8	26.96	ND	11.09
71		3.92	>35	>8.9	27.40	ND	13.3								

https://doi.org/10.1021/acs.jmedchem.1c00696
J. Med. Chem. 2021, 64, 9431−9443

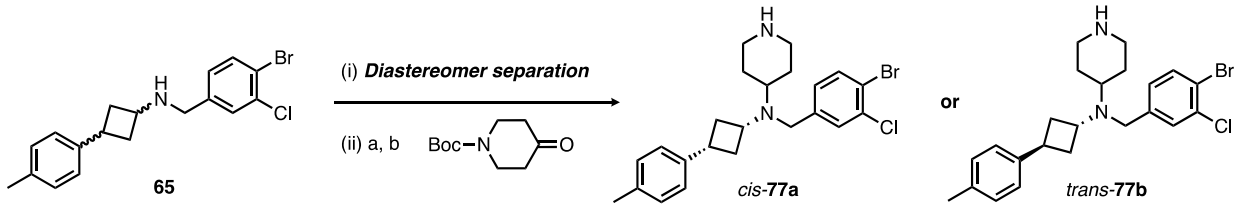

Figure 5. Diastereomer separation and synthesis of *cis*-77**a** and *trans*-77**b**. (a) Preparative diastereomeric separation of *cis*-**65a** and *trans*-**65b** (see the Supporting Information for further details). (b) AcOH, DCE, 60 °C, then $NaBH(OAc)_3$, RT. (c) 4N HCl/dioxane, RT.

Table 7. Biological Activity of *cis*-77a and *trans*-77b

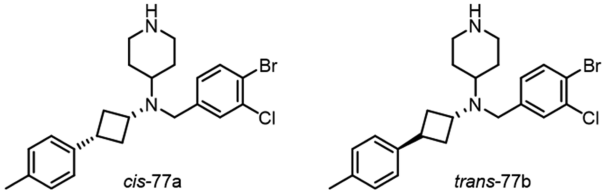

ID	R	EC_{50} (μM)	CC_{50} (μM)	SI	ADME		
					$T_{1/2}$	PAMPA ($1e^{-6}$ cm/s)	Solubility (μg/mL)
77a	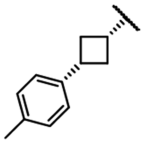	0.325 ± 0.056	4.5	13.8	>30	ND	9.71
77b	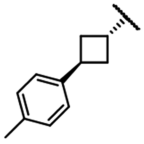	0.047 ± 0.006	3.8 ± 2.8	80.9	>30	ND	1.09

extending to cyclopentyl (**6**) and cyclohexyl (**7**) restores activity to the low μM range. Replacement of the alkylamine linkage for amide **10** or sulfonamide **11** results in total loss of biological activity, so sp^3 linkers at this position were maintained moving forward. Isosteric replacement of the attached phenyl with isomers of pyridine (**12**–**14**) or thiophene (**15**–**16**) did not improve potency, so we next turned to various substituted phenyl analogues (Table 3).

In general, *para*- and *meta*-halogen substitutions within the phenyl "A Ring" (**18**–**21**, **25**–**29**) gave the best improvements in activity. The most potent analogue at this stage **25** (*m*-Cl; EC_{50} = 0.45 μM) also provided a small increase in $T_{1/2}$ (<1–1.6 min); however, this is likely not the predominantly metabolically labile area of the compound, since the vast majority of analogues synthesized had little impact on $T_{1/2}$. Substitution with amides (**32**) or acetanilides (**38**) render the series completely inactive (>35 μM).

As the preference for halogen-substituted phenyls was noted in the first round of structural optimization, several di substituted halogen-containing analogues were prepared to probe these observed trends in search of additional potency improvements (Table 4). This exercise proved fruitful and led to the identification of **40** (*p*-Br, *m*-Cl; EC_{50} = 0.21 μM), the most potent compound at this stage, approximately a 10-fold increase in potency over hit **2** (EC_{50} = 2.09 μM).

Following incubation with rat liver microsome lysates, a mass spectrometry-based metabolite identification study revealed major structural fragments corresponding to oxidative cleavage at the benzylic position on the linker "C" (Figure 3). This led us to the assumption that by modifying both the linker "C" and "D" ring substituents, we may be able to positively impact the metabolic stability of the compound. Thus, we first turned to the linker and several analogues were synthesized with modifications in this region (Table 5a).

With the exception of the vicinal cyclobutane derivative **54**, modifications in this linker region were found to unilaterally increase the metabolic $T_{1/2}$ of the series; notably, the introduction of the isopropyl moiety in compound **50** increased the $T_{1/2}$ by approximately 10-fold from 2.6 min (**40**) to 23.3 min. Compound **55**, with a 1,3-cyclobutyl linker, retains similar potency and toxicity profiles to **40**; however, the half-life has been increased from 2.6 to 12.3 min. Importantly, the marked increases in $T_{1/2}$ when modifying linker "C" is concordant with the identification of this area of the molecule as a primary metabolic hotspot.

Substitutions off the "D" ring phenyl (Table 5b, **56**–**63**) were chosen based on retaining the broader physicochemical properties of the molecule; substituents such as amides and anilides were excluded based on the previous SAR results. Several "D" ring modifications were also found to increase $T_{1/2}$ to levels appropriate for *in vivo* studies, as well as further increases in potency. Notably, *p*-methyl derivative **56** is the most potent analogue identified with an EC_{50} of 75 nM (approximately 30-fold more potent than **2**) and an *in vitro* metabolic $T_{1/2}$ of >30 min (the maximum half-life in this assay).[3]

Finally, SAR about the piperidine ring area was explored while carrying through optimal substitutions in other areas of

https://doi.org/10.1021/acs.jmedchem.1c00696
J. Med. Chem. 2021, 64, 9431–9443

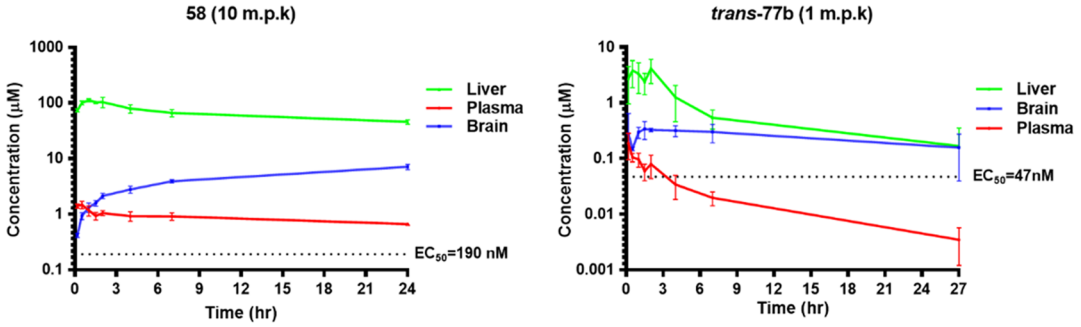

	Compound 58 (10 mg/kg)			Compound 77b (1.0 mg/kg)		
	Plasma	Liver	Brain	Plasma	Liver	Brain
AUC_{last} (hr*ng/mL)	10500	793000	56800	275	9570	3000
AUC_{Last}/D (hr*kg*ng/mL/mg	1050	79300	5680	275	9570	3000
$T_{1/2}$ (h)	ND	ND	ND	7.3	6.7	ND
T_{max} (h)	0.5	1	24	0.167	2	1.5
C_{max} (ng/mL; μM)	759; 1.48	57400; 112	3630; 7.08	84.7; 0.189	1850; 4.13	153; 0.342
C_{max}/D (kg*ng/mL/mg)	75.9	5740	363	84.7	1850	153
AUC_{last} ratio (Tissue/Plasma)	/	76	5.4	/	35	11

Figure 6. Pharmacokinetic analysis of compounds **58** and *trans*-**77b** in mice at 10 and 1 mg/kg, respectively. AUC_{last} = Area under curve out to last time point of measurement. AUC_{last}/D = AUC_{last} divided by dose to permit a comparison between **58** and *trans*-**77b**. $T_{1/2}$ ND = not determined due to excessively long clearance time. T_{max} = Time-point maximum concentration reached. C_{max} Concentration at T_{max}.

the molecule (Table 6). N- to O-substitution and N-acylation were not tolerated (**66**, **67**); however, alkylation of piperidine nitrogen (**68**, **69**), changes to ring size, structure, and addition of bridging carbons (**70**−**76**) yields a series of analogues with low micromolar potency, minimal cytotoxicity, and favorable *in vitro* ADME parameters. Previously identified unsubstituted piperidine **56** remains the most potent compound in the entire series with a notably long *in vitro* $T_{1/2}$.

As such, **56** was synthesized as its constitutive *cis*- *trans*-isomers about the cyclobutyl linker (Figure 5; Table 7). This was accomplished via synthesis and chiral separation of *cis*-**65** and *trans*-**65**; subsequent reductive amination with Boc-protected piperidine-4-one and deprotection gave *cis*-**77a** and *trans*-**77b**. The *trans*-isomer **77b** was identified as the more active diastereomer with an EC_{50} = 47 nM and maintained $T_{1/2}$ > 30 min, representing the most promising analogue identified in the medicinal chemistry campaign.

Pharmacokinetic Studies. Prior to the completion of the SAR campaign, a preliminary mouse pharmacokinetic (PK) study was performed with compound **58**, as it represented the most promising analogue at the time. The goals of this study were to validate the *in vitro* ADME data, ascertain any qualitative *in vivo* toxicity that may need to be addressed, and develop dosing parameters for future *in vivo* efficacy studies based on tissue-specific distribution and clearance. Compound **58** was formulated as its oxalate salt (1:1) in water with 30% (w/v) hydroxypropyl-*β*-cyclodextrin (HP*β*CD), solubilized at 2 mg/mL, and administered at 10 mg/kg (IP) equivalent to a dosage of approximately 0.813 mg/kg in humans[35] (Table 7). Following administration, maximum concentration (C_{max}) is reached in 0.5 h in plasma and 1 h in the liver. The C_{max} in the liver is approximately 100-fold of that reached in plasma and over 500-fold of the *in vitro* EC_{50} (C_{max} liver and plasma: 112 and 1.5 μM respectively; EC_{50} = 0.19 μM). No unusual behavior or acute toxicity (posture, body temperature, respiratory rate, etc.) was noted in the course of the study (24 h). The elimination phase of the drug in all compartments analyzed (plasma, liver, brain) was quite slow, which resulted in an unquantifiable $T_{1/2}$. Total exposure calculations (AUC) show that a distribution of **58** was preferential to liver vs plasma, by a factor of **76**.

Upon completion of the SAR study, purified diastereomer *trans*-**77b** emerged as the most potent analogue, with an EC_{50} of 47 nM and >4-fold increased selectivity index (Figure 6), compared to the previously *in vivo* administered compound **58**. Lead compound **77b** was formulated as its di-HCl salt in a mixture of 10% PEG-300 and water containing 20% (w/v) hydroxypropyl-*β*-cyclodextrin (HP*β*CD). Given the favorable distribution to the liver and slow clearance of compound **58**, we lowered the dose to 1 mg/kg. Similar to **58**, compound **77b** reached C_{max} quickly in both plasma (0.167 h) and liver (2 h) with concentrations of 0.189 μM (∼4x-EC_{50}) and 4.13 μM (∼88x-EC_{50}), respectively. Clearance from the plasma and liver displayed $T_{1/2}$ of 7.3 and 6.7 h, respectively. Preferential liver distribution was observed with 35-fold AUC values vs plasma. Importantly, there was once again no observed toxicity throughout the course of the study, resulting in a very promising PK profile for our most active HCV inhibitor at a single administered low-dose regimen.

CONCLUSIONS

In summary, we report the discovery and optimization of a new series of HCV inhibitors with a novel mechanism of action, targeting viral assembly, which displays synergy *in vitro* with multiple currently approved HCV therapeutics. Through an extensive medicinal chemistry campaign, the chemotype was optimized to yield several compounds with nanomolar anti-HCV activity, low levels of cytotoxicity, and favorable physicochemical/*in vitro* ADME profiles. Pharmacokinetic studies in mice confirm a promising PK profile and reveal preferential distribution to the liver with a long *in vivo* metabolic $T_{1/2}$. For anti-HCV treatment, liver localization is favorable, allowing appropriate therapeutic concentrations to be reached in the target organ at lower doses. We believe that these results define lead compound **77b** as a promising candidate for *in vivo* efficacy studies and further preclinical development.

https://doi.org/10.1021/acs.jmedchem.1c00696
J. Med. Chem. 2021, 64, 9431−9443

EXPERIMENTAL SECTION

Biology. *Routine Culture.* Human hepatoma cell line Huh7.5.1 was maintained in Dulbecco's modified Eagle's medium (DMEM) (Life Technologies, Grand Island, NY) with 10% fetal bovine serum (FBS) (Life Technologies, Grand Island, NY) and antibiotics in 5% CO_2 at 37 °C. HCV-Luc (HCV JFH-1 strain with insertion of the luciferase reporter gene), HCVsc (single-cycle defective HCV particle), and pseudotyped viruses (HCVpp-1a, HCVpp-1b) were produced as previously reported.

HCV-Luc Infection and ATPlite Assays. Huh7.5.1 cells were plated in white, flat bottomed 96-well plates at 10^4 cells/well and incubated overnight. The cells were infected with HCV-Luc in the presence of increasing concentrations of the compound of interest. The viral level was measured 48 h after treatment using a Renilla luciferase assay system (Promega, Madison, WI). ATP-based cell viability assay was carried out in parallel to evaluate the cytotoxicity with an ATPlite assay kit (PerkinElmer, Waltham, MA). The concentration values that led to 50% viral inhibition and cytotoxicity (EC_{50} and CC_{50}, respectively) were calculated using the nonlinear regression equation in GraphPad Prism 5.0 software (GraphPad Software Inc., La Jolla, CA).

HCV Replication Cycle Assays. In the HCVsc assay, Huh7.5.1 cells were cultured in 96-well plates (10^4 cells/well) overnight before infection with HCVsc in the presence of the compound of interest. After 48 h of incubation, the viral level was detected by a luciferase assay. In the HCV subgenomic replicon assay, HCV replicon (GT 2a) cells were plated into 96-well plates at 10^4 cells/well and incubated overnight. The cells were treated with tested compounds for 48 h, and luciferase activity was measured. In HCVpp assays, Huh7.5.1 cells were seeded in 96-well plates (10^4 cells/well) and cultured overnight. Then, the cells were infected with HCVpp GT 1a, 1b, for 4 h in the presence of the compound. The cells were then washed and cultured for 48 h followed by a luciferase assay to detect the HCV entry. Positive controls (cyclosporin A at 10 μM and bafilomycin A1 at 10 nM) were tested in parallel.

Immunofluorescence and Lipid Droplet Staining. Huh7.5.1 cells were fixed with 4% paraformaldehyde (ChemCruz, Dallas, TX) 48−72 h after HCV (JFH1) infection for HCV core protein staining. For permeabilization, 0.5% Triton X-100 (Tx-100, Sigma-Aldrich, St Louis, MO) in phosphate-buffered saline (PBS) was used. Then, the cells were blocked by 3% bovine serum albumin (BSA, Sigma-Aldrich, St. Louis, MO) in PBS. For HCV core protein staining, in-house anticore antibody was used as a primary antibody and Alexa Fluor 488 goat antimouse IgG (Invitrogen, Carlsbad, CA) or Alexa Fluor 555 donkey antimouse IgG (Invitrogen, Carlsbad, CA) was applied as a secondary antibody. For lipid droplet staining for colocalization of HCV core protein and lipid droplet, 1 mg/mL BODIPY493/503 (Thermo Fisher Scientific, Waltham, MA) is treated to the cells at 1:1000 dilution in PBS. The cells were then incubated for 30 min and were followed by 4′,6-diamidino-2- phenylindole dilactate (DAPI, Invitrogen, Carlsbad, CA) nuclei staining. Images were captured by a Zeiss LSM 700 confocal microscope and are shown in Supplemental Figure 1. The colocalization signal was analyzed by ImageJ (National Institutes of Health, Bethesda, MD). For normalization of colocalization signal intensity, colocalization signal intensity was divided by HCV core signal intensity.

Pharmacokinetics/ADME. *Rat Liver Microsomal Stability Assay.* Multiple time-point metabolic stability assay was run in triplicates using the substrate depletion method or the *in vitro* half-life ($T_{1/2}$) method. Sample analysis and half-life determinations were performed using a previously described method.[22]

Aqueous Kinetic Solubility Assay. Pion's patented μSOL assay for kinetic solubility determination was used. In this assay, the classical saturation shake-flask solubility method was adapted to a 96-well microtiter plate format and a cosolvent method with *n*-propanol as the reference compound was utilized. Test compounds were prepared in 10 mM dimethyl sulfoxide (DMSO) solutions (45 μL) and diluted with the cosolvent to a final drug concentration of 150 μM in the aqueous solution (pH 7.4). Samples were incubated at room temperature for 6 h to achieve equilibrium. The samples were then filtered to remove any precipitate formed. The concentration of the compound in the filtrate was measured by UV absorbance. The reference drug concentration of 17 μM was used for the quantitation of unknown.

Parallel Artificial Membrane Permeability Assay (PAMPA). The effective permeability of compounds was determined via passive diffusion using the stirring double-sink parallel artificial membrane permeability assay (PAMPA) method from pION Inc. (www.pion-inc.com), with a fully automated system of sample preparation, sample analysis, and data processing, as described previously.[23]

Mice Pharmacokinetics. Male CD-1 mice (∼35 g) were obtained from Charles River Laboratories (Wilmington, MA). Mice were housed at the centralized animal facilities at the National Institutes of Health (NIH, Bethesda, MD) with a 12 h light/dark cycle. The housing temperature and relative humidity were monitored based on the Standard Operating Procedure issued by NIH Division of Veterinary Resources (DVR). The animals had free access to water and food. All experimental procedures were approved by the Animal Care and Use Committee of the NIH DVR. The dosing solution of a test compound was freshly prepared prior to the drug administration in 50% propylene glycol and 50% water. The pharmacokinetics was evaluated after single administration at the stated dosage and route (i.e., oral gavage [PO], intravenous [IV], or intraperitoneal [IP] injection). The blood and liver samples were collected at predose, 0.083, 0.25, 0.5, 1, 2, 4, 7, and 24 h. Three animals (n = 3) were sacrificed at each time point, and blood and liver samples were collected. Plasma samples were harvested after centrifugation of blood samples at room temperature. Plasma and liver samples were frozen immediately after collection and stored at −80 °C prior to sample analysis. The concentrations of a test compound in the plasma and liver were determined by ultraperformance liquid chromatography-mass spectrometry analysis (UPLC-MS/MS). The mean concentrations from three animals at each time point were used in the PK calculation. The pharmacokinetic parameters were calculated using the noncompartmental method (Model 200 for oral or IP administration and Model 201 for IV administration) of the pharmacokinetic software package Phoenix WinNonlin, version 6.2 (Certara, St. Louis, MO). The area under the plasma and liver concentration vs time curve (AUC) was calculated using the linear trapezoidal method. Where warranted, the slope of the apparent terminal phase was estimated by log linear regression using at least 3 data points, and the terminal rate constant (λ) was derived from the slope. AUC0-∞ was estimated as the sum of the AUC0-t (where t is the time of the last measurable concentration) and C_t/λ. The apparent terminal half-life ($t_{1/2}$) was calculated as $0.693/\lambda$. The oral bioavailability was estimated from the dose-normalized AUC ratio between IV and oral administration. The maximum concentration (C_{max}) and time to reach C_{max} (T_{max}) were also reported.

Chemistry. All air or moisture-sensitive reactions were performed under a positive pressure of nitrogen, using oven- or flame-dried glassware where stated. Anhydrous solvents were purchased from Sigma-Aldrich (St. Louis, MO). "Normal-phase chromatography" refers to automated purification using a Tyledyne ISCO CombiFlash Rf+ with preloaded silica gel RedisepRF GOLD flash columns of an appropriate size. "Reverse phase chromatography" refers to purification performed on a Waters semipreparative HPLC system (Waters Corp., Milford, MA) with a Phenomenex Luna C18 (5 μm, 30 × 75 mm^2; Phenomenex, Inc., Torrance, CA) at a flow rate of 45.0 mL/min. The mobile phase consisted of acetonitrile and water, each containing 0.1% trifluoroacetic acid, with a gradient of 10−50% acetonitrile over 8 min. Automated fraction collection was triggered by UV detection at 220 nM or manually, where low UV absorbance was noted. Analytical analysis was performed on an Agilent LC/MS (Agilent Technologies, Santa Clara, CA) with a Phenomenex Luna C18 column (3 μm, 3 × 75 mm^2) at a temperature of 50 °C.

Purity determination and reaction progress monitoring were performed using an Agilent diode array detector for both Method 1 (final analytical gradients) and Method 2 (reaction progress monitoring). The purity of all final compounds was confirmed to

https://doi.org/10.1021/acs.jmedchem.1c00696
J. Med. Chem. 2021, 64, 9431−9443

be ≥95%. Retention time (^{t}R) and m/z $(M + H)^+$ are reported. In some cases, adducts such as (M + Na, M + H_2O) are observed exclusively and are reported as such:

Method 1: A 7 min gradient of 4−100% acetonitrile (containing 0.025% trifluoroacetic acid) in water.

It (containing 0.05% trifluoroacetic acid) was used at a flow rate of 1.0 mL/min.

Method 2: A 3 min gradient of 4−100% acetonitrile (containing 0.025% trifluoroacetic acid) in water.

It (containing 0.05% trifluoroacetic acid) was used at a flow rate of 1.0 mL/min.

High-resolution mass spectrometric analysis was performed on final compounds using an Agilent 6130 mass spectrometer with electrospray ionization in positive mode.

^{1}H NMR and ^{13}C NMR spectra were recorded on Varian-400 spectrometers (400 MHz for ^{1}H and 101 or 151 MHz for ^{13}C; Agilent Technologies; Santa Clara, CA). Signals are described as singlets (s), broad singlets (bs), doublets (d), triplets (t), quadruplets (q), multiplets (m), broad multiplets (bm), doublet of doublets (dd), and doublet of triplets (dt). Spectra were analyzed using MestReNova. For compounds that were isolated as a mixture of diastereomers, the spectra are reported as recorded without additional interpretation of integration or peak count.

Chiral chromatographic analysis and purification was performed on Agilent 1200 series HPLC using a ChiralCel OJ column, 5 × 50 cm^2, at a compound concentration of 20 mM, using a mobile phase of hexanes/EtOH/MeOH/diethylamine (50:25:25:0.1), and a flow rate of 40 mL/min.

Synthesis. General Procedure A (standard reductive amination and Boc-deprotection of crude amine): To a solution of amine (50 mg, 1 equiv) in dichloroethane (0.5 mL) was added an aldehyde (2 equiv) followed by sodium triacetoxyborohydride (1.6 equiv). The reaction was stirred at room temperature overnight. The reaction was quenched with $NaHCO_3$ (3 mL) and extracted with EtOAc (2 × 4 mL). The combined organics were removed by blowing down under a stream of nitrogen at 40 °C. The crude material was stirred with HCl (2 mL, 4 M in dioxane) for 2 h at room temperature, after which the mixture was concentrated by blowing a stream of nitrogen at 40 °C. The crude product was dissolved in DMSO and purified by reverse phase chromatography to give the desired amine.

General Procedure B (displacement of primary alkyl bromides): To a solution of 4 (60 mg, 1 equiv) in ACN (1 mL) was added 2-bromobenzyl bromide (1.1 equiv) followed by K_2CO_3 (3 equiv). The reaction was stirred at room temperature overnight. The reaction was diluted with brine (3 mL) and EtOAc (4 mL), organics were separated, and the aqueous phase was extracted with EtOAc (2 × 4 mL). Combined organics were blown down under a stream of nitrogen. To the resultant crude oil was added HCl (2 mL, 4 M in dioxane). The reaction was stirred for 2 h at room temperature, then blown down under N_2. The crude material was dissolved in DMSO and purified by reverse phase chromatography to give the desired amine.

General Procedure C (amide analogues): To a solution of **4** (500 mg, 1 equiv) in dichloroethane (DCE) (8 mL) was added the appropriate formylbenzoic acid (370 mg, 1.5 equiv) followed by sodium triacetoxyborohydride (557 mg, 1.5 equiv). The reaction was stirred at room temperature overnight. Volatiles were removed by blowing down under a stream of nitrogen at 40 °C. The crude material was dissolved in DMF (6 mL) with sonication and a 2 mL aliquot was removed and added to a new reaction vessel (approx 0.5 mmol of intermediate). To this was added HATU (347 mg, 1.8 equiv) and the resulting solution was stirred for 10 min at room temperature. The appropriate amine (93 mg, 2.3 equiv) was added followed by *N*,*N*-diisopropylethylamine (0.119 mL, 1.5 equiv). The mixture was stirred overnight at room temperature. The reaction was quenched with $NaHCO_3$ (3 mL) and extracted with EtOAc (2 × 4 mL). The combined organics are removed by blowing down under a stream of nitrogen at 40 °C. The resulting Boc-protected intermediate was stirred with HCl (3 mL, 4 M in dioxane) for 2 h. The reaction mixture was concentrated by blowing down under a stream of nitrogen at 40 °C. The crude material was dissolved in a DMSO and purified by reverse phase column chromatography to give the desired amide.

General Method D (reductive amination with heating for imine formation): To a solution of amine (0.05 g, 1 equiv) in DCE (0.5 mL) was added a mixture of ketone (1.2 equiv) and acetic acid (1 equiv). The mixture was heated to 60 °C for 1 h, after which sodium triacetoxyborohydride (1.5 equiv). The mixture was allowed to cool to rt and stirred overnight. The reaction mixture was then blown down with N_2(g) at 50 °C and further concentrated under reduced pressure. The crude material was taken up in DCM (5 mL), solids were removed via vacuum filtration, and the filtrate was purified via normal-phase flash chromatography to give the desired product.

General Method E (Boc-deprotection): Boc-protected amine (20−75 mg) was taken up in HCl (2 M in ether, 1 mL) and stirred at rt for 1−3 h under N_2(g). The mixture was then blown down with N_2(g) at rt and further concentrated under reduced pressure to give the desired amine.

*N-Benzyl-N-phenethylpiperidin-4-amine, 2TFA (**2**).* General Method A (**4** and benzaldehyde) to give **2** (63 mg, 0.120 mmol, 73% yield). ^{1}H NMR (DMSO-d_6) δ 11.65 (s, 1H), 9.47 (d, J = 9.3 Hz, 1H), 9.35 (q, J = 9.8 Hz, 1H), 7.82 (dd, J = 6.5, 3.0 Hz, 2H), 7.51−7.40 (m, 3H), 7.28 (t, J = 7.2 Hz, 2H), 7.21 (t, J = 7.3 Hz, 1H), 7.11 (d, J = 6.9 Hz, 2H), 4.52 (dd, J = 13.1, 3.9 Hz, 1H), 4.35 (dd, J = 13.1, 7.0 Hz, 1H), 3.77−3.65 (m, 1H), 3.40 (d, J = 10.4 Hz, 2H), 3.15 (t, J = 13.5 Hz, 3H), 3.01−2.79 (m, 3H), 2.43 (t, J = 14.9 Hz, 2H), and 2.25 (dt, J = 20.2, 12.6 Hz, 2H). ^{1}H NMR *Freebase* (DMSO-d_6) δ 7.48−6.89 (m, 10H), 3.73−3.63 (m, 2H), 3.10−2.84 (m, 2H), 2.68−2.48 (m, J = 8.0 Hz, 5H), 2.36 (t, J = 11.7 Hz, 2H), 1.59 (d, J = 11.3 Hz, 2H), and 1.34 (d, J = 10.5 Hz, 2H). ^{13}C NMR (DMSO-d_6) δ 137.42, 131.89, 130.75, 129.87, 129.07, 128.99, 127.28, 58.12, 53.87, 50.60, 42.32, 30.07, 23.06, and 22.95. LCMS (Method 2), ^{t}R = 3.15 min, m/z 295.2 $[M + H]^+$. HRMS m/z calcd for $[M + H]^+$ 295.2169, found 295.2161.

*tert-Butyl 4-(phenethylamino)piperidine-1-carboxylate (**4**).* To a solution of *tert*-butyl 4-aminopiperidine-1-carboxylate (5 g, 24.97 mmol) and 2-phenylacetaldehyde (3.15 g, 26.2 mmol) in MeOH (45 mL) was added acetic acid (0.143 mL, 2.497 mmol). After 15 min, sodium cyanoborohydride (2.353 g, 37.4 mmol) was added in three portions. The resulting solution was stirred at rt for 30 min and then partitioned between ethyl acetate and water. The separated organic layer was washed with brine, dried over $MgSO_4$, and concentrated in vacuo. The crude material was purified by normal-phase chromatography (100%) EtOAc to yield *tert*-butyl 4-(phenethylamino)-piperidine-1-carboxylate (6.23 g, 20.47 mmol, 82% yield) as a yellow oil.

^{1}H NMR ($CDCl_3$) δ 7.37−7.25 (m, 2H), 7.23−7.08 (m, 3H), 4.01 (s, 2H), 2.91 (dd, J = 8.1, 6.8 Hz, 2H), 2.86−2.67 (m, 4H), 2.62 (tt, J = 10.5, 3.9 Hz, 1H), 1.98 (s, 1H), 1.86−1.76 (m, 2H), 1.43 (s, 9H), and 1.30−1.16 (m, 2H). ^{13}C NMR ($CDCl_3$) δ 154.67, 139.22, 128.84, 128.61, 128.53, 128.29, 126.36, 79.48, 55.02, 47.59, 42.30, 35.76, 31.69, and 28.39. LCMS (Method 2), ^{t}R = 2.78 min, m/z 305.1. HRMS m/z calcd for $[M + Na]^+$ 327.2043, found 327.2028.

*N-Phenethyl-N-(piperidin-4-yl)benzamide, TFA (**10**).* To a solution of *tert*-butyl 4-(phenethylamino)piperidine-1-carboxylate (60 mg, 0.197 mmol) in DCM (0.5 mL) was added benzoyl chloride (0.027 mL, 0.237 mmol) followed by triethylamine (0.060 mL, 0.434 mmol) and DMAP (2.408 mg, 0.020 mmol) at room temperature. The reaction was stirred overnight, and the solvent was removed under nitrogen. Boc-deprotection and purification was carried out in an analogous manner to general procedure A, yielding *N*-phenethyl-*N*-(piperidin-4-yl)benzamide. ^{1}H NMR (400 MHz, DMSO-d_6) δ 8.63 (s, 1H), 8.34 (s, 1H), 7.44 (dd, J = 5.0, 1.9 Hz, 3H), 7.37−7.31 (m, 2H), 7.21 (d, J = 18.0 Hz, 4H), 6.83 (s, 1H), 4.23 (s, 1H), 3.52 (s, 2H), 3.31 (d, J = 15.5 Hz, 3H), 2.78 (d, J = 48.4 Hz, 3H), 2.25 (s, 1H), and 1.81 (d, J = 68.1 Hz, 3H). ^{13}C NMR (151 MHz, DMSO-d_6) δ 161.10, 142.33, 141.19, 140.54, 139.80, 132.49, 131.58, 129.52, 129.10, 117.23, 56.71, 54.07, 51.61, 46.33, 45.63, 39.34, 37.68, 29.51, and 29.05. LCMS (Method 2) ^{t}R = 3.83 min, m/z 309.2. HRMS m/z calcd for $[M + H]^+$ 309.1961, found 309.1957.

https://doi.org/10.1021/acs.jmedchem.1c00696
J. Med. Chem. 2021, 64, 9431−9443

*N-(3-Chlorobenzyl)-N-phenethylpiperidin-4-amine, 2TFA (**25**).* General Method A (**4** and 3-chlorobenzaldehyde) to give **25**. ^{1}H NMR (400 MHz, DMSO-d_6) δ 9.05 (d, J = 11.5 Hz, 1H), 8.73 (d, J = 11.5 Hz, 1H), 7.70 (s, 1H), 7.56−7.43 (m, 3H), 7.28 (dd, J = 8.1, 6.6 Hz, 2H), 7.24−7.18 (m, 1H), 7.17−7.11 (m, 2H), 4.38 (s, 2H), 3.66 (s, 1H), 3.44 (d, J = 12.5 Hz, 2H), 3.16 (t, J = 8.5 Hz, 2H), 2.98 (q, J = 12.1 Hz, 2H), 2.86 (s, 2H), 2.26 (d, J = 12.8 Hz, 2H), and 1.98 (dd, J = 18.9, 8.4 Hz, 2H). ^{13}C NMR (101 MHz, DMSO-d_6) δ 159.25, 133.90, 131.11, 129.80, 129.08, 127.29, 115.34, 57.88, 53.28, 51.07, 42.57, 30.41, and 23.60. LCMS (Method 2) ^{t}R = 3.50 min m/z 329.2. HRMS m/z calcd for $[M + H]^+$ 329.1779, found 329.1767.

*N-(4-Bromo-3-chlorobenzyl)-N-phenethylpiperidin-4-amine, 2TFA (**40**).* General Method A (**4** and 4-bromo-3-chlorobenzaldehyde) to give **40**. ^{1}H NMR (600 MHz, DMSO-d_6) δ 8.29−6.79 (m, 8H), 3.88 (d, J = 278.1 Hz, 4H), 3.28 (d, J = 115.5 Hz, 3H), 2.86 (d, J = 47.3 Hz, 4H), and 2.30−1.45 (m, 4H). ^{13}C NMR (151 MHz, DMSO-d_6) δ 161.24, 137.01, 135.98, 134.70, 133.29, 131.81, 131.57, 129.80, 116.84, 60.63, 55.30, 53.82, 45.43, 32.67, and 26.12. LCMS (Method 2) ^{t}R = 3.79 min, m/z 407.1. HRMS m/z calcd for $[M + H]^+$ 407.0884, found 407.0899.

*tert-Butyl 4-((4-bromo-3-chlorobenzyl)amino)piperidine-1-carboxylate (**49**).* General Method D (*tert*-butyl 4-oxopiperidine-1-carboxylate and (4-bromo-3-chlorophenyl)methanamine) to give **49**. ^{1}H NMR (400 MHz, DMSO-d_6) δ 7.66 (d, J = 8.2 Hz, 1H), 7.58 (d, J = 2.0 Hz, 1H), 7.23 (dd, J = 8.2, 2.0 Hz, 1H), 3.77 (d, J = 13.2 Hz, 2H), 3.68 (s, 2H), 2.76 (s, 2H), 1.73 (dd, J = 12.9, 3.7 Hz, 2H), 1.36 (s, 9H), and 1.19−1.03 (m, 2H). LCMS (Method 1) ^{t}R = 2.83 min, m/z 405.1.

*N-(4-Bromo-3-chlorobenzyl)-N-(3-phenylcyclobutyl)piperidin-4-amine, 2HCl (**55**).* General Method D (**49** and 3-phenylcyclobutan-1-one) followed by General Method E to give **55**. ^{1}H NMR (600 MHz, DMSO-d_6) δ 10.63 (s, 1H), 8.90 (s, 1H), 8.64 (s, 1H), 7.84 (d, J = 48.1 Hz, 2H), 7.48 (s, 1H), 7.34−7.24 (m, 2H), 7.25−7.10 (m, 3H), 4.31 (d, J = 44.5 Hz, 2H), 4.00 (s, 1H), 3.62 (s, 2H), 3.39 (s, 3H), 3.08 (s, 1H), 2.94 (s, 2H), 2.68 (s, 1H), 2.16 (d, J = 52.6 Hz, 3H), and 1.95 (s, 2H).^{13}C NMR (151 MHz, DMSO) δ 161.31, 145.86, 137.13, 136.04, 134.67, 131.58, 131.40, 129.67, 126.05, 117.01, 59.60, 56.11, 53.57, 46.30, 45.17, 38.96, 35.10, and 26.69. LCMS (Method 2) ^{t}R = 3.76 min, m/z 435.1. HRMS m/z calcd for $[M + H]^+$ 435.1020, found 435.1025.

*N-(4-Bromo-3-chlorobenzyl)-N-(3-(p-tolyl)cyclobutyl)piperidin-4-amine (**56**), 2HCl.* General Method D (49 and 3-(*p*-tolyl)-cyclobutan-1-one) followed by General Method E to give **56**. ^{1}H NMR (400 MHz, Chloroform-d) δ 7.55−7.45 (m, 2H), 7.20−7.00 (m, 4H), 3.60 (d, J = 6.3 Hz, 2H), 3.47−3.28 (m, 1H), 3.13 (d, J = 12.3 Hz, 2H), 3.01 (td, J = 10.0, 5.0 Hz, 1H), 2.62 (td, J = 11.8, 5.9 Hz, 1H), 2.53 (td, J = 12.0, 2.3 Hz, 2H), 2.39 (qd, J = 10.1, 8.8, 2.7 Hz, 2H), 2.32 (d, J = 9.4 Hz, 3H), 2.18 (tt, J = 8.4, 4.0 Hz, 1H), 1.89 (dt, J = 13.1, 9.7 Hz, 2H), 1.69 (d, J = 12.5 Hz, 2H), and 1.45 (dtd, J = 21.5, 10.7, 9.2, 4.0 Hz, 2H). ^{13}C NMR (101 MHz, $CDCl_3$) δ 143.90, 141.97, 135.37, 133.99, 133.20, 133.18, 129.65, 129.59, 129.04, 128.91, 127.38, 127.26, 126.58, 126.36, 119.74, 77.33, 77.01, 76.69, 57.55, 57.48, 53.67, 52.27, 49.88, 49.57, 46.53, 37.01, 35.01, 32.73, 32.62, 29.92, 20.96, and 20.95. LCMS (Method 2) ^{t}R = 4.39 min, m/z 447.0. HRMS m/z calcd for $[M + H]^+$ 449.1177, found 449.1166.

*N-(4-Bromo-3-chlorobenzyl)-N-(3-(4-bromophenyl)cyclobutyl)-piperidin-4-amine (**58**), 2HCl.* General Method D (**49** and 3-(4-bromophenyl)cyclobutan-1-one) followed by General Method E to give **58**. ^{1}H NMR (400 MHz, Chloroform-d) δ 7.54−7.44 (m, 2H), 7.39 (ddd, J = 14.5, 8.5, 2.1 Hz, 2H), 7.16−6.95 (m, 3H), 3.59 (dd, J = 9.1, 1.8 Hz, 2H), 3.46−3.25 (m, 1H), 3.12 (d, J = 11.8 Hz, 2H), 2.99 (td, J = 9.8, 7.3 Hz, 1H), 2.60 (td, J = 11.9, 2.8 Hz, 1H), 2.53 (t, J = 12.2 Hz, 2H), 2.46−2.31 (m, 2H), 2.23 (s, 2H), 2.20−2.09 (m, 1H), 1.86 (tdd, J = 10.9, 6.9, 2.5 Hz, 2H), and 1.53−1.38 (m, 2H). ^{13}C NMR (101 MHz, $CDCl_3$) δ 143.89, 143.63, 134.05, 133.24, 133.22, 131.35, 131.23, 129.61, 129.51, 128.48, 128.23, 127.32, 127.17, 119.85, 119.53, 77.30, 57.45, 57.38, 53.46, 52.19, 49.89, 49.53, 46.43, 36.86, 34.86, 32.63, 32.57, and 29.75. LCMS (Method 2) ^{t}R = 4.16 min, m/z 512.9. HRMS m/z calcd for $[M + H]^+$ 513.0125, found 513.0137.

*Separation of **65** into Respective cis-(65a) trans-(65b) Diastereomers.* Five hundred milligrams of **65**, a mixture of diastereomers, was separated via chiral liquid chromatography using a ChiralCel OJ column, 5 × 50 cm^2, at a concentration of 20 μM using a mobile phase of hexane/EtOH/MeOH/DEA (50:25:25:0.1) and a flow rate of 40 mL/min. This gave *cis-N*-(4-bromo-3-chlorobenzyl)-3-(*p*-tolyl)cyclobutan-1-amine, **65a**, 263.6 mg, colorless oil, ^{t}R = 7.88 min, ee = 95.7% and *trans-N*-(4-bromo-3-chlorobenzyl)-3-(*p*-tolyl)-cyclobutan-1-amine, **65b**, 211.8 mg pale yellow oil, ^{t}R = 6.85 min, ee > 98%.

*cis-N-(4-Bromo-3-chlorobenzyl)-3-(p-tolyl)cyclobutan-1-amine (**65a**).* ^{1}H NMR (400 MHz, Chloroform-d) δ 7.55 (d, J = 8.2 Hz, 1H), 7.46 (d, J = 2.0 Hz, 1H), 7.18−7.04 (m, 5H), 3.70 (s, 2H), 3.24 (tt, J = 8.7, 6.8 Hz, 1H), 3.09 (tt, J = 10.1, 7.7 Hz, 1H), 2.68 (tdd, J = 9.9, 6.1, 2.6 Hz, 2H), 2.32 (s, 3H), and 1.78 (dtd, J = 10.1, 8.7, 2.8 Hz, 2H). LCMS (Method 2) ^{t}R = 4.67 min, m/z 366.0.

*trans-N-(4-Bromo-3-chlorobenzyl)-3-(p-tolyl)cyclobutan-1-amine (**65b**).* ^{1}H NMR (400 MHz, Chloroform-d) δ 7.55 (d, J = 8.2 Hz, 1H), 7.46 (d, J = 2.0 Hz, 1H), 7.17−7.08 (m, 6H), 3.69 (s, 2H), 3.59 (ddd, J = 15.4, 9.5, 5.9 Hz, 1H), 3.53−3.42 (m, 1H), 2.43−2.34 (m, 2H), 2.33 (s, 3H), and 2.29−2.18 (m, 2H). LCMS (Method 2) ^{t}R = 4.77 min, m/z 366.0.

*cis-N-(4-Bromo-3-chlorobenzyl)-N-(3-(p-tolyl)cyclobutyl)-piperidin-4-amine, 2HCl (**77a**).* To a mixture of *tert*-butyl 4-oxopiperidine-1-carboxylate (0.060 g, 0.302 mmol) and *cis-N*-(4-bromo-3-chlorobenzyl)-3-(*p*-tolyl)cyclobutan-1-amine (**65a**) (0.1 g, 0.274 mmol) in DCE (1.371 mL) was added sodium triacetoxyborohydride (0.087 g, 0.411 mmol) followed by AcOH (0.016 mL, 0.274 mmol). The reaction vessel was sealed and stirred overnight at rt. The reaction mixture was diluted with DCM (50 mL) and the organic phase was washed with NaOH (1 M; 1 × 30 mL) and brine (1 × 30 mL), dried over $MgSO_4$, filtered, and concentrated to give a colorless oil. Crude Boc-protected intermediate was purified via normal-phase flash chromatography (0−10% EtOAc in DCM), to give Boc-protected intermediate as a dark yellow oil (0.095 g, 0.173 mmol). The material was taken up in HCl (2 M in ether; 1.0 mL) and stirred for 3 h at rt. The resulting slurry was blown down with N_2(g) at rt. The crude material was purified via normal-phase flash chromatography (DIOL; 0−20% MeOH in DCM) to give **77a** (91 mg, 0.175 mmol, 63.8% yield) as a white solid. ^{1}H NMR (400 MHz, Chloroform-d) δ 9.71 (s, 1H), 9.49 (s, 1H), 7.64−7.55 (m, 2H), 7.30−7.23 (m, 1H), 7.15−7.06 (m, 4H), 3.92 (s, 2H), 3.59−3.46 (m, 2H), 3.44 (s, 1H), 3.37 (s, 1H), 3.03 (q, J = 8.8 Hz, 1H), 2.89 (s, 2H), 2.38 (s, 4H), 2.30 (s, 3H), and 2.15 (d, J = 15.3 Hz, 4H). ^{13}C NMR (101 MHz, Chloroform-d) δ 162.44, 162.08, 136.37, 135.16, 134.29, 131.31, 129.16, 126.61, 117.96, 77.19, 56.05, 53.15, 50.88, 43.53, 36.07, 32.75, 24.07, and 20.96. LCMS (Method 2) ^{t}R = 4.22 min, m/z 447.1. HRMS m/z calcd for $[M + H]^+$ 447.1124, found 447.1184.

*trans-N-(4-Bromo-3-chlorobenzyl)-N-(3-(p-tolyl)cyclobutyl)-piperidin-4-amine, 2HCl (**77b**).* To a mixture of *tert*-butyl 4-oxopiperidine-1-carboxylate (0.060 g, 0.302 mmol) and *trans-N*-(4-bromo-3-chlorobenzyl)-3-(*p*-tolyl)cyclobutan-1-amine (**65b**) (0.1 g, 0.274 mmol) in DCE (1.371 mL) was added sodium triacetoxyborohydride (0.087 g, 0.411 mmol) followed by AcOH (0.016 mL, 0.274 mmol). The reaction vessel was sealed and stirred overnight at rt. The reaction mixture was diluted with DCM (50 mL) and the organic phase was washed with NaOH (1 M; 1 × 30 mL) and brine (1 × 30 mL), dried over $MgSO_4$, filtered, and concentrated to give a colorless oil. Crude Boc-protected intermediate was purified via normal-phase flash chromatography (0−15% EtOAc in DCM), to give Boc-protected intermediate as an off-white solid (0.079 g, 0.144 mmol). The material was taken up in HCl (2 M in ether; 1.0 mL) and stirred for 3 h at rt. The resulting slurry was blown down with N_2(g) at rt. The crude material was purified via normal-phase flash chromatography (DIOL; 0−20% MeOH in DCM) to give **77b** (67 mg, 0.129 mmol, 47.1% yield) as a white solid. ^{1}H NMR (400 MHz, DMSO-d_6) δ 8.17 (s, 2H), 7.71 (d, J = 8.2 Hz, 1H), 7.60 (d, J = 2.0 Hz, 1H), 7.30

https://doi.org/10.1021/acs.jmedchem.1c00696
J. Med. Chem. 2021, 64, 9431−9443

(dd, J = 8.3, 2.0 Hz, 1H), 7.18 (d, J = 8.1 Hz, 2H), 7.12 (d, J = 7.9 Hz, 2H), 3.66 (s, 2H), 3.72−3.60 (m, 1H), 3.25 (d, J = 12.4 Hz, 2H), 2.85−2.72 (m, 3H), 2.33 (dt, J = 12.0, 9.3 Hz, 2H), 2.27 (s, 3H), 2.11 (ddd, J = 12.3, 8.2, 3.1 Hz, 2H), 1.74 (d, J = 12.6 Hz, 2H), and 1.64−1.50 (m, 2H). ^{13}C NMR (101 MHz, DMSO-d_6) δ 144.90, 142.84, 134.99, 133.96, 133.23, 129.72, 129.36, 128.50, 126.93, 119.37, 54.70, 53.21, 48.84, 43.85, 35.00, 32.44, 25.84, and 21.01. LCMS (Method 2) ^{t}R = 4.26 min, m/z 447.1. HRMS m/z calcd for $[M + H]^+$ 447.1124, found 447.1186.

■ ASSOCIATED CONTENT

Supporting Information

The Supporting Information is available free of charge at https://pubs.acs.org/doi/10.1021/acs.jmedchem.1c00696.

Molecular formula string table (CSV)

Chemistry and biology protocols; compound **2** disrupts the colocalization of HCV core proteins and lipid droplets as determined by immunofluorescence, representative examples are shown; characterization of all additional newly synthesized compounds; and chiral analysis of **65a** and **65b** (PDF)

■ AUTHOR INFORMATION

Corresponding Author

Juan J. Marugan − *Division of Pre-Clinical Innovation, National Center for Advancing Translational Sciences, National Institutes of Health, Rockville, Maryland 20850, United States;* orcid.org/0000-0002-3951-7061; Phone: 301-480-9857; Email: maruganj@mail.nih.gov

Authors

Adam Rolt − *Liver Diseases Branch, National Institute of Diabetes and Digestive and Kidney Diseases, National Institutes of Health, Bethesda, Maryland 20892, United States;* Present Address: Department of Biochemistry, University of Oxford, Oxford OX1 3QU, U.K.

Daniel C. Talley − *Division of Pre-Clinical Innovation, National Center for Advancing Translational Sciences, National Institutes of Health, Rockville, Maryland 20850, United States*

Seung Bum Park − *Liver Diseases Branch, National Institute of Diabetes and Digestive and Kidney Diseases, National Institutes of Health, Bethesda, Maryland 20892, United States*

Zongyi Hu − *Liver Diseases Branch, National Institute of Diabetes and Digestive and Kidney Diseases, National Institutes of Health, Bethesda, Maryland 20892, United States*

Andrés Dulcey − *Division of Pre-Clinical Innovation, National Center for Advancing Translational Sciences, National Institutes of Health, Rockville, Maryland 20850, United States*

Christopher Ma − *Liver Diseases Branch, National Institute of Diabetes and Digestive and Kidney Diseases, National Institutes of Health, Bethesda, Maryland 20892, United States*

Parker Irvin − *Liver Diseases Branch, National Institute of Diabetes and Digestive and Kidney Diseases, National Institutes of Health, Bethesda, Maryland 20892, United States*

Madeleine Leek − *Liver Diseases Branch, National Institute of Diabetes and Digestive and Kidney Diseases, National Institutes of Health, Bethesda, Maryland 20892, United States*

Amy Q. Wang − *Division of Pre-Clinical Innovation, National Center for Advancing Translational Sciences, National Institutes of Health, Rockville, Maryland 20850, United States*

Andrew V. Stachulski − *The Robert Robinson Laboratories, Department of Chemistry, University of Liverpool, Liverpool L69 7ZD, U.K.*

Xin Xu − *Division of Pre-Clinical Innovation, National Center for Advancing Translational Sciences, National Institutes of Health, Rockville, Maryland 20850, United States*

Noel Southall − *Division of Pre-Clinical Innovation, National Center for Advancing Translational Sciences, National Institutes of Health, Rockville, Maryland 20850, United States*

Marc Ferrer − *Division of Pre-Clinical Innovation, National Center for Advancing Translational Sciences, National Institutes of Health, Rockville, Maryland 20850, United States*

T. Jake Liang − *Liver Diseases Branch, National Institute of Diabetes and Digestive and Kidney Diseases, National Institutes of Health, Bethesda, Maryland 20892, United States*

Complete contact information is available at: https://pubs.acs.org/10.1021/acs.jmedchem.1c00696

Author Contributions

$^{\perp}$A.R. and D.C.T. contributed equally to this work. The manuscript was written through the contributions of all authors. All authors have given approval to the final version of the manuscript.

Notes

The authors declare no competing financial interest.

■ ABBREVIATIONS

ACN, acetonitrile; AcOH, acetic acid; EtOAc, ethyl acetate; EtOH, ethanol; HATU, 1-[bis(dimethylamino)methylene]-1*H*-1,2,3-triazolo[4,5-*b*]pyridinium 3-oxid hexafluorophosphate; MeOH, methanol; $MgSO_4$, magnesium sulfate; $NaHCO_3$, sodium bicarbonate; NaOH, sodium hydroxide; HCl, hydrochloric acid

■ REFERENCES

(1) Blach, S.; et al. Global prevalence and genotype distribution of hepatitis C virus infection in 2015: a modelling study. *Lancet Gastroenterol. Hepatol.* **2017**, *2*, 161−176.

(2) WHO Global Hepatitis Report, 2017. https://www.who.int/hepatitis/publications/global-hepatitis-report2017/en/.

(3) Kish, T.; Aziz, A.; Sorio, M. Hepatitis C in a new era: A review of current therapies. *Pharm. Ther.* **2017**, *42*, 316−329.

(4) Abergel, A.; Asselah, T.; Metivier, S.; Kersey, K.; Jiang, D.; Mo, H.; Pang, P. S.; Samuel, D.; Loustaud-Ratti, V. Ledipasvir-sofosbuvir in patients with hepatitis C virus genotype 5 infection: an open-label, multicentre, single-arm, phase 2 study. *Lancet Infect. Dis.* **2016**, *16*, 459−464.

(5) Abergel, A.; Metivier, S.; Samuel, D.; Jiang, D.; Kersey, K.; Pang, P. S.; Svarovskaia, E.; Knox, S. J.; Loustaud-Ratti, V.; Asselah, T. Ledipasvir plus sofosbuvir for 12 weeks in patients with hepatitis C genotype 4 infection. *Hepatology* **2016**, *64*, 1049−1056.

(6) Afdhal, N.; Zeuzem, S.; Kwo, P.; Chojkier, M.; Gitlin, N.; Puoti, M.; Romero-Gomez, M.; Zarski, J. P.; Agarwal, K.; Buggisch, P.; Foster, G. R.; Brau, N.; Buti, M.; Jacobson, I. M.; Subramanian, G. M.; Ding, X.; Mo, H.; Yang, J. C.; Pang, P. S.; Symonds, W. T.;

McHutchison, J. G.; Muir, A. J.; Mangia, A.; Marcellin, P. Ledipasvir and sofosbuvir for untreated HCV genotype 1 infection. *N. Engl. J. Med.* **2014**, *370*, 1889−1898.
(7) Gane, E. J.; Hyland, R. H.; An, D.; Svarovskaia, E.; Pang, P. S.; Brainard, D.; Stedman, C. A. Efficacy of ledipasvir and sofosbuvir, with or without ribavirin, for 12 weeks in patients with HCV genotype 3 or 6 infection. *Gastroenterology* **2015**, *149*, 1454−1461.
(8) Feld, J. J.; Moreno, C.; Trinh, R.; Tam, E.; Bourgeois, S.; Horsmans, Y.; Elkhashab, M.; Bernstein, D. E.; Younes, Z.; Reindollar, R. W.; Larsen, L.; Fu, B.; Howieson, K.; Polepally, A. R.; Pangerl, A.; Shulman, N. S.; Poordad, F. Sustained virologic response of 100% in HCV genotype 1b patients with cirrhosis receiving ombitasvir/paritaprevir/r and dasabuvir for 12 weeks. *J. Hepatol.* **2016**, *64*, 301−307.
(9) Ferenci, P.; Bernstein, D.; Lalezari, J.; Cohen, D.; Luo, Y.; Cooper, C.; Tam, E.; Marinho, R. T.; Tsai, N.; Nyberg, A.; Box, T. D.; Younes, Z.; Enayati, P.; Green, S.; Baruch, Y.; Bhandari, B. R.; Caruntu, F. A.; Sepe, T.; Chulanov, V.; Janczewska, E.; Rizzardini, G.; Gervain, J.; Planas, R.; Moreno, C.; Hassanein, T.; Xie, W.; King, M.; Podsadecki, T.; Reddy, K. R. ABT-450/r-ombitasvir and dasabuvir with or without ribavirin for HCV. *N. Engl. J. Med.* **2014**, *370*, 1983−1992.
(10) Sulkowski, M. S.; Eron, J. J.; Wyles, D.; Trinh, R.; Lalezari, J.; Wang, C.; Slim, J.; Bhatti, L.; Gathe, J.; Ruane, P. J.; Elion, R.; Bredeek, F.; Brennan, R.; Blick, G.; Khatri, A.; Gibbons, K.; Hu, Y. B.; Fredrick, L.; Schnell, G.; Pilot-Matias, T.; Tripathi, R.; Da Silva-Tillmann, B.; McGovern, B.; Campbell, A. L.; Podsadecki, T. Ombitasvir, paritaprevir co-dosed with ritonavir, dasabuvir, and ribavirin for hepatitis C in patients co-infected with HIV-1: a randomized trial. *JAMA* **2015**, *313*, 1223−1231.
(11) Vernaz, N.; Girardin, F.; Goossens, N.; Brügger, U.; Riguzzi, M.; Perrier, A.; Negro, F. Drug pricing evolution in hepatitis C. *PLoS One* **2016**, *11*, No. e0157098.
(12) Ward, J. W.; Hinman, A. R. What is needed to eliminate hepatitis B virus and hepatitis C virus as global health threats. *Gastroenterology* **2019**, *156*, 297−310.
(13) Jia, J.; Zhu, F.; Ma, X.; Cao, Z. W.; Li, Y. X.; Chen, Y. Z. Mechanisms of drug combinations: interaction and network perspectives. *Nat. Rev. Drug Discovery* **2009**, 111−128.
(14) Delang, L.; Vliegen, I.; Froeyen, M.; Neyts, J. Comparative study of the genetic barriers and pathways towards resistance of selective inhibitors of hepatitis C virus replication. *Antimicrob. Agents Chemother.* **2011**, *55*, 4103−4113.
(15) He, S.; Lin, B.; Chu, V.; Hu, Z.; Hu, X.; Xiao, J.; Wang, A. Q.; Schweitzer, C. J.; Li, Q.; Imamura, M.; Hiraga, N.; Southall, N.; Ferrer, M.; Zheng, W.; Chayama, K.; Marugan, J. J.; Liang, T. J. Repurposing of the antihistamine chlorcyclizine and related compounds for treatment of hepatitis C virus infection. *Sci. Transl. Med.* **2015**, *7*, No. 282ra49.
(16) He, S.; Xiao, J.; Dulcey, A. E.; Lin, B.; Rolt, A.; Hu, Z.; Hu, X.; Wang, A. Q.; Xu, X.; Southall, N.; Ferrer, M.; Zheng, W.; Liang, T. J.; Marugan, J. J. Discovery, optimization, and characterization of novel chlorcyclizine derivatives for the treatment of hepatitis C virus infection. *J. Med. Chem.* **2016**, *59*, 841−853.
(17) Rolt, A.; Le, D.; He, S.; Hu, Z.; Liang, T. J.; Wang, A. Q.; Dulcey, A. E.; Hughes, E.; Marugan, J. J.; Singleton, M.; Shah, P.; Xu, X.; Chayama, K.; Imamura, M.; Uchida, T. Preclinical pharmacological development of chlorcyclizine derivatives for the treatment of hepatitis C virus infection. *J. Infect. Dis.* **2018**, *217*, 1761−1769.
(18) He, S.; Li, K.; Lin, B.; Hu, Z.; Xiao, J.; Hu, X.; Wang, A. Q.; Xu, X.; Ferrer, M.; Southall, N.; Zheng, W.; Aubé, J.; Schoenen, F. J.; Marugan, J. J.; Liang, T. J.; Frankowski, K. J. Development of an aryloxazole class of hepatitis C virus inhibitors targeting the entry stage of the viral replication cycle. *J. Med. Chem.* **2017**, *60*, 6364−6383.
(19) Ma, C. D.; Imamura, M.; Talley, D. C.; Rolt, A.; Xu, X.; Wang, A. Q.; Le, D.; Uchida, T.; Osawa, M.; Teraoka, Y.; Li, K.; Hu, X.; Park, S. B.; Chalasani, N.; Irvin, P. H.; Dulcey, A. E.; Southall, N.; Marugan, J. J.; Hu, Z.; Chayama, K.; Frankowski, K. J.; Liang, T. J. Fluoxazolevir inhibits hepatitis C virus infection in humanized chimeric mice by blocking viral membrane fusion. *Nat. Microbiol.* **2020**, *5*, 1532−1541.
(20) Hu, Z.; Rolt, A.; Hu, X.; Ma, C. D.; Le, D. J.; Park, S. B.; Houghton, M.; Southall, N.; Anderson, D. E.; Talley, D. C.; Lloyd, J. R.; Marugan, J. C.; Liang, T. J. Chlorcyclizine inhibits viral fusion of hepatitis C virus entry by directly targeting HCV envelope glycoprotein 1. *Cell Chem. Biol.* **2020**, *27*, 780−792.
(21) Goldwasser, J.; Cohen, P. Y.; Lin, W.; Kitsberg, D.; Balaguer, P.; Polyak, S. J.; Chung, R. T.; Yarmush, M. L.; Nahmias, Y. Naringenin inhibits the assembly and long-term production of infectious hepatitis C virus particles through a PPAR-mediated mechanism. *J. Hepatol.* **2011**, *55*, 963−971.
(22) Qu, X.; Pan, X.; Weidner, J.; Yu, W.; Alonzi, D.; Xu, X.; Butters, T.; Block, T.; Guo, J. T.; Chang, J. Inhibitors of endoplasmic reticulum alpha-glucosidases potently suppress hepatitis C virus virion assembly and release. *Antimicrob. Agents Chemother.* **2011**, *55*, 1036−1044.
(23) Cheng, Y.-L.; Lan, K.-H.; Lee, W.-P.; Tseng, S.-H.; Hung, L.-R.; Lin, H.-C.; Lee, F.-Y.; Lee, S.-D.; Lan, K.-H. Amiodarone inhibits the entry and assembly steps of hepatitis C virus life cycle. *Clin. Sci.* **2013**, *125*, 439.
(24) Kota, S.; Takahashi, V.; Ni, F.; Snyder, J. K.; Strosberg, A. D. Direct binding of a hepatitis C Virus inhibitor to the viral capsid protein. *PLoS One* **2012**, *7*, No. e32207.
(25) Duvignaud, J. B.; Majeau, N.; Delisle, P.; Voyer, N.; Gagne, S. M.; Leclerc, D. Interfering with hepatitis C virus assembly in vitro using affinity peptides directed towards core protein. *Can. J. Microbiol.* **2012**, *58*, 475−482.
(26) Hu, Z.; Hu, X.; He, S.; Yim, H. J.; Xiao, J.; Swaroop, M.; Tanega, C.; Zhang, Y.-q.; Yi, G.; Kao, C. C.; Marugan, J.; Ferrer, M.; Zheng, W.; Southall, N.; Liang, T. J. Identification of novel anti-hepatitis C virus agents by a quantitative high throughput screen in a cell-based infection assay. *Antiviral Res.* **2015**, *124*, 20−29.
(27) PubChem qHTS assay for inhibitors of hepatitis C virus (HCV). https://pubchem.ncbi.nlm.nih.gov/bioassay/651820#section=Top.
(28) PubChem qHTS assay for inhibitors of hepatitis C virus (HCV): Confirmation assay for cherry-picked compounds. https://pubchem.ncbi.nlm.nih.gov/bioassay/720575.
(29) Bartosch, B.; Cosset, F. L. Studying HCV cell entry with HCV pseudoparticles (HCVpp). *Methods Mol. Biol.* **2009**, *510*, 279−293.
(30) Hu, Z.; Lan, K.-H.; He, S.; Swaroop, M.; Hu, X.; Southall, N.; Zheng, W.; Liang, T. J. Novel cell-based hepatitis C virus infection assay for quantitative high-throughput screening of anti-hepatitis C virus compounds. *Antimicrob. Agents Chemother.* **2014**, *58*, 995.
(31) Barba, G.; Harper, F.; Harada, T.; Kohara, M.; Goulinet, S.; Matsuura, Y.; Eder, G.; Schaff, Z.; Chapman, M. J.; Miyamura, T.; Bréchot, C. Hepatitis C virus core protein shows a cytoplasmic localization and associates to cellular lipid storage droplets. *Proc. Natl. Acad. Sci. U.S.A.* **1997**, *94*, 1200−1205.
(32) Lindenbach, B. D.; Rice, C. M. The ins and outs of hepatitis C virus entry and assembly. *Nat. Rev. Microbiol.* **2013**, *11*, 688−700.
(33) Lin, B.; He, S.; Yim, H. J.; Liang, T. J.; Hu, Z. Evaluation of antiviral drug synergy in an infectious HCV system. *Antiviral Ther.* **2016**, *21*, 595−603.
(34) Hu, Z.; Lan, K.-H.; He, S.; Swaroop, M.; Hu, X.; Southall, N.; Zheng, W.; Liang, T. J. Novel cell-based hepatitis C virus infection assay for quantitative high-throughput screening of anti-hepatitis C virus compounds. *Antimicrob. Agents Chemother.* **2014**, *58*, 995−1004.
(35) Nair, A. B.; Jacob, S. A simple practice guide for dose conversion between animals and human. *J. Basic Clin. Pharm.* **2016**, *7*, 27−31.

https://doi.org/10.1021/acs.jmedchem.1c00696
J. Med. Chem. 2021, 64, 9431−9443